is so similar to variation 1 that it is not reproduced. The only significant difference is that the main peak (E,F) resembles the experimental peak even more closely in that F is the stronger component, with E appearing as a slightly weaker low-frequency shoulder.

For the difference bands, we can only present the theoretical results, since there are no experimental data. It can be seen that for each model, variations 1 and 2 lead to strikingly different results. This in itself fully justifies separate presentation of these data. Obviously, experimental observation of these difference spectra would provide a very useful way of fixing the relative magnitudes of the parameters a, b, etc., in the polarizability tensor. This problem could also be usefully examined by more precise measurements on the 300°K Stokes spectra. In addition, it would be interesting to have low-temperature data available to compare with our predicted spectra; conceivably these would show more fine detail. In all cases, it is obviously desirable that the intensities be measured by some strictly linear recorder.

PHYSICAL REVIEW VOLUME 179, NUMBER 3 15 MARCH 1969

F Center in Cesium Fluoride: Optical Absorption Properties*

T. A. FULTON† AND D. B. FITCHEN
Laboratory of Atomic and Solid State Physics, Cornell University, Ithaca, New York 14850
(Received 7 November 1968)

Studies of the well-resolved triplet line shape of the F band in cesium fluoride and its temperature dependence, magnetic circular dichroism, and stress-induced behavior are reported. The results are in accord with the picture proposed by Moran, in which the triplet structure results from a combined spin-orbit coupling and Jahn-Teller effect in the excited states, although an accurate numerical calculation of the line shape predicted by his adiabatic model shows certain features not found experimentally. The circular-dichroism results show that the contribution of the Γ_{1g} lattice modes to the F-band second moment is $\approx 15\%$. This relatively weak coupling, taken along with the spin-orbit stabilization of the Γ_{3g} and Γ_{5g} mode interactions, results in the component bands of the line shape being quite narrow. These narrow bands are comparable in width to optical-phonon energies in cesium fluoride, so that discrete optical-phonon transitions are observed in the F band.

I. INTRODUCTION

THE F center, an electron trapped at a negative ion vacancy in an ionic crystal, has been an object of investigation for many years, particularly in the alkali halides. Much of the work has concerned the prominent optical absorption band (F band) lying in or near the visible region of the spectrum. This band arises from transitions from the S-like ground state to a P-like set of excited states and, typically, has an oscillator strength >0.5. It is relatively broad, ~ 0.2 eV at 0°K, and is nearly Gaussian in shape in the commonly studied alkali halides such as KCl, KBr, or NaCl.

The nature of the states of the F center is of interest because the potential binding the electron is provided solely by the host lattice ions, in contrast to localized states based on impurities. Consequently, the coupling of the electronic states to the ionic motion is strong and the states of the center are vibronic, involving both electronic and nuclear coordinates. This strong electron-lattice coupling is responsible for the breadth and featureless shape of the F band and presents theoretical treatments with substantial difficulties.

Experimentally, extracting much information about the states of the F center from the relatively featureless F band is a difficult task. A number of advances in these studies have been made in the last few years, however, particularly in three areas. First, several revealing experiments on the response of the F band to applied perturbations have been performed. Of particular interest are the Faraday rotation studies of Mort, Lüty, and Brown,[1] the magnetic circular dichroism studies of Margerie and Romestain,[2,3] of Gareyte and d'Aubigne,[4] and of Henry,[5] and the stress-induced dichroism studies of Schnatterly.[6] A particularly useful contribution was made by Henry, Schnatterly, and Slichter[7] (HSS hereafter), who developed a theoretical analysis relating

* Work supported primarily by the U. S. Atomic Energy Commission under Contract No. AT (30-1)-3464, Technical Report No. NYO-3464-14, and also by the Alfred P. Sloan Foundation. The Advanced Research Projects Agency is also acknowledged for the use of the central facilities of the Materials Science Center at Cornell University, MSC Report No. 996.

† Present address: Bell Telephone Laboratories, Murray Hill, N. J. 07974.

[1] J. Mort, F. Lüty, and F. C. Brown, Phys. Rev. **137**, A566 (1965).
[2] J. Margerie and R. Romestain, Compt. Rend. **258**, 4490 (1964).
[3] R. Romestain and J. Margerie, Compt. Rend. **258**, 2525 (1964).
[4] J. Gareyte and Y. Merle D'Aubigne, Compt. Rend. **258**, 6393 (1964).
[5] C. H. Henry, Phys. Rev. **140**, A256 (1965).
[6] S. E. Schnatterly, Phys. Rev. **140**, A1364 (1965).
[7] C. H. Henry, S. E. Schnatterly, and C. P. Slichter, Phys. Rev. **137**, A583 (1965).

the moments of the F band and the changes in moments caused by applied perturbations, such as stress, to the properties of the P-like excited states and their interaction with the vibrations of the host lattice. Application of their results to a number of the previously mentioned experiments have yielded much information about the spin-orbit coupling in the excited P-like states and the relative strengths of the electron-lattice coupling of these states with the cubic, tetragonal, and trigonal vibrational modes of the lattice.

Another promising technique is that of Raman scattering from F centers, first studied by Worlock and Porto.[8] This method may eventually become the most detailed experimental source of information about the electron-phonon coupling in the F center. A partial basis for theoretical interpretation of the experiments has been given by Henry.[9]

A third avenue of approach was opened by the discovery of Rabin and Schulman[10] of structure in the low-temperature F bands of CsBr, an unresolved doublet, and of CsCl, a barely resolved triplet. This was followed by the finding of a well-resolved triplet in the F band of CsF by Hughes and Rabin[11] and a doublet structure in the low-temperature F band of CsI by Lynch[12] (see Fig. 1).

After some initial uncertainty as to the sources of the structure, circular dichroism studies of Margerie and Romestain[2] revealed that for CsBr and CsCl the structure was related to a large spin-orbit coupling in the P-like states, giving a spin-orbit splitting$\approx F$-band width. A moments analysis by HSS of these experiments indicated that the coupling of the noncubic (tetragonal and trigonal) modes of vibration, i.e., the Jahn-Teller effect, is also important in determining the shape of the F band in CsBr and CsCl. A model which takes explicit account of the interplay between the spin-orbit coupling and the cubic and noncubic lattice vibrations was subsequently used by Moran[13] to explain and fit the line shapes for all four cesium halides, both doublets and triplets.

Although all of these studies give related and complementary information about the nature of the F center, the cesium-halide studies are particularly intriguing because the spin-orbit coupling and the Jahn-Teller effects, which are common to all F centers, play a very visible and important role in the cesium halides. In this way the cesium-halide F bands are important both for the information they reveal about F centers and as examples of a particular variety of optical centers in solids, namely, as model examples of spin-orbit-Jahn-Teller interplay.

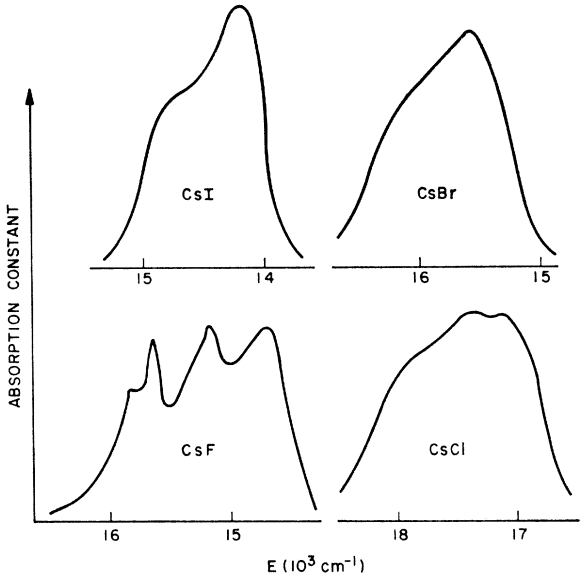

FIG. 1. F bands of the cesium halides. That of CsF is from the present work. The others are after Ref. 13.

The F band of the F center in CsF possesses much better-resolved structure than any of the other alkali-halide F centers (Fig. 1) and thus presents a promising target for study. In addition to possessing an attractive line shape the CsF F center is of interest as a case of extreme host lattice properties. CsF has the largest alkali-to-halide ion-size ratio (1.86–1.16 Å) and mass ratio (133–19 a.m.u.) of any of the alkali halides. Further, CsF alone of the cesium halides has an NaCl crystal structure in common with the rest of the alkali halides, allowing a more direct comparison of its properties with those of the more commonly studied alkali halides.

Despite the attractive nature of the CsF F center the only previous reported work on the system is the original work of Hughes and Rabin.[11] The present work reports part of an extensive further study of the CsF F center. The approach used in this study was to investigate a number of different properties of the CsF F center and to attempt to correlate these in order to form an over-all picture of the nature of the F center in this material.[14] Measurements were made concerning the optical absorption at low temperatures, the temperature dependence of the absorption, and its circular dichroism induced at low temperatures by a magnetic field. In addition, experiments involving the hydrostatic pressure shift of the F band and qualitative experiments on the uniaxial-stress-induced dichroism were performed. Experiments related to the relaxed excited state including photoconductivity, luminescence, and ground-state repopulation will be described in a subsequent publication.

[8] J. M. Worlock and S. P. S. Porto, Phys. Rev. Letters **15**, 697 (1965).
[9] C. H. Henry, Phys. Rev. **152**, 699 (1966).
[10] H. Rabin and J. H. Schulman, Phys. Rev. **120**, 2007 (1960).
[11] F. Hughes and H. Rabin, J. Phys. Chem. Solids **24**, 586 (1963).
[12] D. W. Lynch, Phys. Rev. **127**, 1537 (1962).
[13] P. R. Moran, Phys. Rev. **137**, A1016 (1965).
[14] T. A. Fulton, thesis, Cornell University (unpublished). Additional details of the present work, particularly the experimental aspects, are available in this thesis.

The picture emerging from these measurements is in general accord with that suggested by Moran.[13] The center is found to exhibit a large spin-orbit splitting in its excited P-like states and to possess a relatively strong coupling of these states to noncubic lattice vibrations and a much weaker coupling to cubic vibrations, an effect also observed for static strains. These interactions conspire to permit observation of discrete phonon transitions in the F band, a previously unobserved feature.

In addition, the F band of CsF provides an interesting example of effects which can occur in a situation in which spin-orbit and Jahn-Teller couplings of comparable strength are simultaneously present. Its behavior provides a direct demonstration of properties which are important but not easily observed for other F centers.

In Sec. II the theory needed to understand the experiments, primarily due to HSS and Moran, will be sketched. Section III describes the experiments and presents the resulting data. Section IV gives an analysis of the data and discusses its implications. Section V is a summary of the work.

II. THEORY

A. HSS Treatment

The related models of HSS and of Moran may be used to explain much of the behavior observed in the CsF F band. This section sketches their treatments, emphasizing some qualitative aspects which play a particularly important role in the CsF F center.

HSS base their treatment on a Hamiltonian

$$H=H_e+H_{\mathrm{SO}}+H_{\mathrm{L}}+H_{e\mathrm{L}}+H_{\mathrm{P}}, \tag{1}$$

where $H_e=p_e^2/2m_e+V(r_e)$ describes a one-electron system with an attractive potential $V(r_e)$ which is cubically symmetric, i.e., transforms according to Γ_{1g} in the symmetry group O_h appropriate to the F center. H_e has eigenstates $|0\rangle|m\rangle$, $|x\rangle|m\rangle$, $|y\rangle|m\rangle$, and $|z\rangle|m\rangle$, where $|m\rangle$ is the spinor $|\frac{1}{2}\rangle$ or $|-\frac{1}{2}\rangle$; $|0\rangle$ is the ground electronic state of H_e, having Γ_{1g} ("S-like") symmetry with energy E_0; and $|x\rangle$, $|y\rangle$, and $|z\rangle$ are a degenerate set of excited electronic states of Γ_{4u} ("P-like") symmetry having energy E_1. We collectively denote the states $|x\rangle|m\rangle$, $|y\rangle|m\rangle$, and $|z\rangle|m\rangle$ by $|i\rangle|m\rangle$. $H_{\mathrm{L}}=\sum_k(P_k^2/2M_k+\frac{1}{2}M_k\omega_k^2Q_k^2)$ describes a harmonic lattice with normal modes labeled by wave vector k, with frequency ω_k and corresponding to momenta P_k and coordinates Q_k. The eigenstates of H_{L} are $|x_l\rangle$. The normal modes may also be characterized by their symmetry in O_h, and we make the usual choice of basis states for those modes transforming according to Γ_{3g} ("tetragonal" modes) as having the symmetry of the functions x^2-y^2 and $3z^2-r^2$ and for modes transforming according to Γ_{5g} ("trigonal" modes) we chose basis states having the symmetries of xy, yz, and zx.

H_{SO} allows for a spin-orbit splitting of the P-like states. The approximation is made that H_{SO} only mixes the $|i\rangle|m\rangle$ with each other, so the appropriate eigenstates of H_e+H_{SO} are $|0\rangle|m\rangle$ with energy E_0, the states

$$\begin{aligned}|\tfrac{1}{2},\tfrac{1}{2}\rangle&=\tfrac{1}{3}\sqrt{3}(|z\rangle|+\tfrac{1}{2}\rangle+[|x\rangle+i|y\rangle]|-\tfrac{1}{2}\rangle),\\ |\tfrac{1}{2},-\tfrac{1}{2}\rangle&=\tfrac{1}{3}\sqrt{3}(-|z\rangle|-\tfrac{1}{2}\rangle+[|x\rangle-i|y\rangle]|+\tfrac{1}{2}\rangle),\end{aligned} \tag{2a}$$

with energy $E_1-\lambda$, and the states

$$\begin{aligned}|\tfrac{3}{2},\tfrac{3}{2}\rangle&=-\tfrac{1}{2}\sqrt{2}(|x\rangle+i|y\rangle)|+\tfrac{1}{2}\rangle,\\ |\tfrac{3}{2},\tfrac{1}{2}\rangle&=\tfrac{1}{3}\sqrt{3}[\sqrt{2}|z\rangle|+\tfrac{1}{2}\rangle-\tfrac{1}{2}\sqrt{2}(|x\rangle+i|y\rangle)|-\tfrac{1}{2}\rangle],\\ |\tfrac{3}{2},-\tfrac{1}{2}\rangle&=\tfrac{1}{3}\sqrt{3}[\sqrt{2}|z\rangle|-\tfrac{1}{2}\rangle+\tfrac{1}{2}\sqrt{2}(|x\rangle-i|y\rangle)|+\tfrac{1}{2}\rangle],\\ |\tfrac{3}{2},-\tfrac{3}{2}\rangle&=+\tfrac{1}{2}\sqrt{2}(|x\rangle-i|y\rangle)|-\tfrac{1}{2}\rangle,\end{aligned} \tag{2b}$$

with energy $E_1+\frac{1}{2}\lambda$, where λ is the spin-orbit parameter. These states are collectively denoted $|j,m_j\rangle$. $H_{e\mathrm{L}}=\sum_k V_k(r_e)Q_k$ is an electron-lattice coupling term taken as linear in the lattice coordinates Q_k with the V_k describing the strength of the coupling to the kth mode. H_{P} describes any external perturbation applied to the system (stress, etc.).

HSS make the approximation that $H_{e\mathrm{L}}$ and H_{P} as well as H_{SO} only mix the states $|i\rangle|m\rangle$ with each other and that the state $|0\rangle|m\rangle$ and any other eigenstates of H_e remain unaffected. From symmetry, the only V_k having nonzero matrix elements between the states $|i\rangle|m\rangle$ are those of Γ_{1g}, Γ_{3g}, and Γ_{5g} symmetries. Modes of other symmetries may be neglected. The matrix elements a_k of the various V_k among the states $|x\rangle$, $|y\rangle$, and $|z\rangle$ fully characterize $H_{e\mathrm{L}}$. The values of the a_k are, or course, interrelated by symmetry via the Wigner-Eckart theorem.

Ideally, given the values of the a_k's, ω_k's, M_k's, λ, E_1, and E_0 one could find the eigenfunctions of H, which would have the form $|g\rangle=\sum_l C_l|0\rangle|m\rangle|x_l\rangle$ with eigenvalues E_g, corresponding to the ground states, and $|f\rangle=\sum_{ilm}D_{ilm}|i\rangle|m\rangle|x_l\rangle$ with eigenvalues E_f corresponding to the excited states. Defining the line shape function as $f(E)=C\alpha(E)/E$, where $\alpha(E)$ is the optical absorption constant as a function of energy and C is a normalizing constant, one has

$$f_\eta(E)=\mathrm{Av}(g)\textstyle\sum_f|\langle f|P_\eta|g\rangle|^2\delta(E_f-E_g-E),$$

where P_η is the dipole operator for light of η polarization and $\mathrm{Av}(g)$ denotes a thermal average in the ground state. Alternatively, given an experimental $f(E)$, one might hope to find a set of values for λ, a_k, etc., which would produce this $f(E)$.

In practice, the problem of finding $|g\rangle$ and $|f\rangle$ for a general H has not been solved. HSS were able to derive expressions concerning the moments of $f(E)$, however, which are exact in their model and are of great utility, as follows.

The moments of $f(E)$ are defined as

$$A_f=\int dE\, f(E)\,, \tag{3a}$$

$$\langle E\rangle_f=\frac{1}{A_f}\int Ef(E)dR\,, \tag{3b}$$

$$\langle E^n\rangle_f=\frac{1}{A_f}\int (E-\langle E\rangle_f)^n f(E)dE. \tag{3c}$$

In the model of HSS,

$$\langle E\rangle_f=E_1-E_0\,, \tag{3d}$$

$$\langle E^2\rangle_f=\langle E^2\rangle_1+\langle E^2\rangle_3+\langle E^2\rangle_5+\tfrac{1}{2}\lambda^2\,, \tag{3e}$$

where $\langle E^2\rangle_1$ depends on the value of the a_k's, ω_k's, and M_k's for the Γ_{1g} lattice modes alone, and similarly for $\langle E^2\rangle_3$ and $\langle E^2\rangle_5$ and the Γ_{3g} and Γ_{5g} modes. Note that the first moment is independent of the strength of H_{eL}, and that the effect of the spin-orbit term on the second moment is simply to add $\frac{1}{2}\lambda^2$, just as in the static lattice, that is, the case in which $H_{eL}=0$.

Now let $f(E)$ and $g(E)$ be the line shape in the absence and presence, respectively, of an applied perturbation, (e.g., stress). Define the moments of $f(E)$ and $g(E)$ as in (3) and let

$$\Delta A=A_f-A_g\,, \tag{3f}$$

$$\Delta\langle E\rangle=\int\left(\frac{f(E)}{A_f}-\frac{g(E)}{A_g}\right)EdE=E_f-E_g\,, \tag{3g}$$

$$\Delta\langle E^n\rangle=\int(E-\langle E\rangle_f)^n\left(\frac{f(E)}{A_f}-\frac{g(E)}{A_g}\right)dE. \tag{3h}$$

Then HSS have shown that $\Delta A=0$ and $\Delta\langle E\rangle$ and $\Delta\langle E^2\rangle$ are independent of the strength of H_{eL}, i.e., equal to the static lattice value. The changes in the higher moments are dependent on the particular type of perturbation and are not generally independent of H_{eL}.

In a special case of interest here let $\langle S_z\rangle$ be the spin polarization induced by application of a magnetic field, and let the subscripts + and − refer to the line shape and moments observed for light of circular polarization propagating along the axis of the magnetic field for the positive and negative senses of the field. Then in this case

$$A_+-A_-=0\,, \tag{4a}$$

$$\Delta\langle E\rangle_+-\Delta\langle E\rangle_-=\lambda(\langle S_z\rangle_+-\langle S_z\rangle_-)\,, \tag{4b}$$

$$\Delta\langle E^2\rangle_+-\Delta\langle E^2\rangle_-=-\tfrac{1}{2}\lambda^2(\langle S_z\rangle_+-\langle S_z\rangle_-)\,, \tag{4c}$$

$$\Delta\langle E^3\rangle_+-\Delta\langle E^3\rangle_-=3[\Delta\langle E\rangle_+-\Delta\langle E\rangle_-]\,[\langle E^2\rangle_1+\tfrac{1}{2}(\langle E^2\rangle_3+\langle E^2\rangle_5+\tfrac{1}{2}\lambda^2)]. \tag{4d}$$

The quantities on the left are readily evaluated by forming the quantity $\Delta f(E)=f_+(E)-f_-(E)$ and calculating its moments with respect to $\langle E\rangle$, the unperturbed centroid of the F band. The use of the method of moments in analyzing the results of a circular dichroism experiment can thus be made to yield the quantities λ, $\langle E^2\rangle_1$, and $\langle E^2\rangle_3+\langle E^2\rangle_5$.

B. Moran Treatment

Although the results of HSS are very useful, a complicated line shape such as occurs in the cesium-halide F centers can not be adequately described by a few low moments. To understand these it is necessary to make approximations in order to compute the line shape from the Hamiltonian (1). A natural approach is the adiabatic approximation, used by Moran.[13] He considers a version of (1) in which the center is subjected to spin-orbit coupling and to electron-lattice interactions with a single Γ_{1g} mode and with a doubly degenerate Γ_{3g} mode. (We consider in Sec. IV the effect of Γ_{5g} modes and more than one Γ_{3g} mode.) H_{eL} is treated adiabatically, i.e., the vibrational mode coordinates are treated as parameters and the electronic problem is solved for eigenfunctions, eigenvalues, and optical transition probabilities for fixed values of the vibrational mode coordinates. The optical line shape function is then computed by assuming a probability distribution of the vibrational mode coordinates corresponding to the zero-point and thermal lattice vibrations. This distribution weights the energies and transition probabilities, giving the line shape.

Explicitly, the Hamiltonian is of the form

$$H_M=H_e+H_{SO}+S\,\mathcal{O}_1+T\,\mathcal{O}_{3a}+Z\,\mathcal{O}_{3b}\,, \tag{5}$$

where H_e and H_{SO} are the same as in (1), and $\mathcal{O}_1$, $\mathcal{O}_{3a}$, and $\mathcal{O}_{3b}$ are the operators

$$\mathcal{O}_1=|x\rangle\langle x|+|y\rangle\langle y|+|z\rangle\langle z|\,,$$
$$\mathcal{O}_{3a}=\sqrt{3}(|x\rangle\langle x|-|y\rangle\langle y|)\,,$$
$$\mathcal{O}_{3b}=2|z\rangle\langle z|-|x\rangle\langle x|-|y\rangle\langle y|\,,$$

so that $S\,\mathcal{O}_1$, $T\,\mathcal{O}_{3a}$ and $Z\,\mathcal{O}_{3b}$ represent strain-energy terms corresponding to distortions of Γ_{1g} symmetry, Γ_{3g} symmetry (x^2-y^2 type), and Γ_{3g} symmetry ($3z^2-r^2$ type). H_M is diagonalized between the states $|j,m_j\rangle$ and $|0\rangle|m\rangle$ and the eigenvalues, eigenfunctions, and transition probabilities are computed as functions of λ, S, Z, and T. For 0°K, S, Z, and T are taken as having Gaussian distributions corresponding to zero-point harmonic oscillator distributions. The second moments of the S, Z, and T distributions are taken as, respectively, W_1^2, $\frac{1}{2}W_3^2$, and $\frac{1}{2}W_3^2$, using Moran's notation. The resulting optical absorption band can have a variety of shapes but always has first moment E_1-E_0 and second moment $W_1^2+2W_3^2+\frac{1}{2}\lambda^2$.

To understand the effects of the interplay of H_{eL} and H_{SO} in Moran's treatment, consider the case for

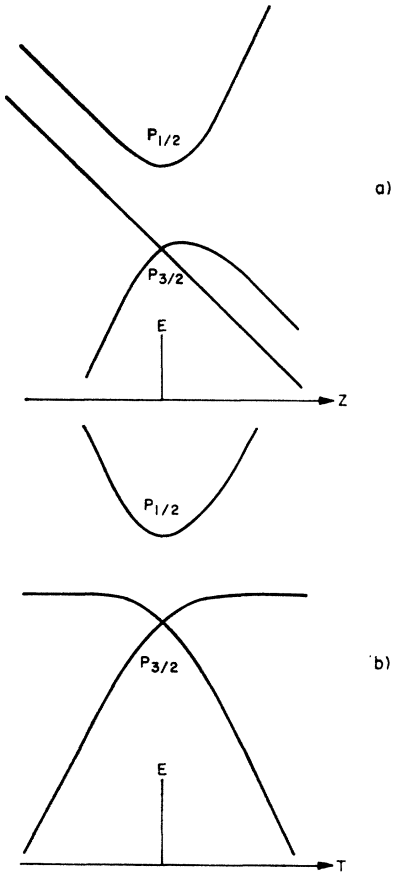

FIG. 2. Cross sections of the energy surfaces as a function of Z and T for (a) $T=0$ and (b) $Z=0$. The full surfaces have C_{3v} symmetry, the curves of (a) and (b) occurring alternately every 60°.

$\lambda=0$. Then for all S, Z, and T the correct eigenfunctions are $|0\rangle|m\rangle$, $|x\rangle|m\rangle$, $|y\rangle|m\rangle$, and $|z\rangle|m\rangle$ with respective energies

$$\begin{aligned}\epsilon_0&=E_0,\\ \epsilon_x&=E_1+S-Z+\sqrt{3}T,\\ \epsilon_y&=E_1+S-Z-\sqrt{3}T,\\ \epsilon_z&=E_1+S+2Z.\end{aligned}\tag{6}$$

These lead to an optical absorption line shape $f(E)$ which is a Gaussian centered at E_1-E_0 with second moment $W_1^2+2W_3^2$.

If the energy surfaces represented by (6) are plotted in Z-T-energy space (letting $S=0$ for the moment) they comprise three infinite planes, each plane corresponding to a pair of eigenfunctions (Kramers degeneracy). Now consider how these surfaces will distort as we set $\lambda\neq 0$. H_{SO} has only off-diagonal nonzero matrix elements between the states $|i\rangle|m\rangle$ so that in regions of the Z-T plane where the energy surfaces are separated by energies $\gg\lambda$ the surfaces will be little distorted. Only near the intersections of the planes will H_{SO} have a substantial effect, and in this region the degeneracies are lifted (save for the point $Z=T=0$ and the unaffected Kramers degeneracy), the surfaces separating along the previous lines of intersection. The resulting surfaces are shown to scale in cross section in the energy-Z and energy-T planes in Figs. 2(a) and 2(b). λ is taken as negative, as is the case for F centers, so that at $Z=T=0$ the upper surface corresponds to the $P_{1/2}$ state and the two lower surfaces to the $P_{3/2}$ state. The appropriate eigenfunctions are the $|j,m_j\rangle$ at the origin and the $|i\rangle|m\rangle$ at large Z and T (except for the directions of intersection in the $\lambda=0$ case) and change continuously between.

For unpolarized light the line shape $f(E)$ for $S=0$, called $f_N(E)$, is constructed by projecting the Gaussian $(1/\pi^{1/2}W_3)\exp[-(Z^2+T^2)/W_3^2]$ onto the energy surfaces. The shape of $f_N(E)$ clearly depends upon the relative values of W_3 and λ. If $\lambda\ll W_3$ the surfaces sampled by Z and T are largely planar and well described by (6), so that $f_N(E)$ remains Gaussian. If, on the other hand $\lambda\gg W_3$, the surfaces sampled by Z and T are near the origin. In this region the upper ($P_{1/2}$) energy surface is nearly flat, so that its contribution will be a narrow band (the $P_{1/2}$ band) at $\approx E_1-E_0-\lambda$. The lower ($P_{3/2}$) surfaces are not flat but are roughly conical near the origin, although the slope is only half that of the slope of the planes for $\lambda=0$. Consequently, the $P_{3/2}$ band is broader than the $P_{1/2}$, although not so broad as the F band for $\lambda=0$ and the same W_3. What is more striking, the static-lattice $P_{3/2}$ energy corresponds only to the point $Z=T=0$. It therefore has zero weight relative to higher and lower energies, so that the $P_{3/2}$ band is a doublet.

Figure 3 shows qualitatively the $f_N(E)$ for the two cases $\lambda\ll W_3$ and $\lambda\gg W_3$. The triplet structure produced in the second case by the combined effects of H_{eL} and H_{SO} is the central result of Moran.

Interesting effects occur in the shape of $f_N(E)$ for the case where $\lambda\approx W_3$, a regime appropriate to the cesium halides. Here Z and T extend to regions in which the energy surfaces are changing between the planar surfaces and the behavior at $Z=T=0$. The $P_{1/2}$ band is asymmetric with a tail to higher energies, since the corresponding energy surface is sharply cut off at the energy $E_1-E_0-\lambda$. The $P_{3/2}$ peaks have a similar asymmetry to lower energy so as to preserve the center of gravity of the total line shape. From the point of view of a perturbation calculation of the effect of small Z and T on the $|j,m_j\rangle$ states, this results from the mixing and repulsion between the $P_{1/2}$ and $P_{3/2}$ states, while the splitting of the $P_{3/2}$ peak into a doublet is interpreted as a similar repulsion between the degenerate $P_{3/2}$ levels.

As previously remarked, for a given W_3 and $\lambda=0$, $f_N(E)$ is Gaussian with second moment $2W_3^2$. As λ is increased, the individual bands become resolved and narrow considerably, as indicated by the flattening of the energy surfaces near the origin. This narrowing

occurs because the states $|j,m_j\rangle$ have zero expectation value for perturbations of Γ_{3g} (or Γ_{5g}) symmetry. The spin-orbit interaction in this way competes with the noncubic electron-lattice terms and causes them to be less effective in broadening the component bands. The effect is most marked for the $P_{1/2}$ band, since the $P_{3/2}$ levels are degenerate in the static lattice, making the off-diagonal noncubic perturbations more effective in shifting these energy levels.

This narrowing effect is quite noticeable in all the cesium-halide F bands (Fig. 1), whose doublet or triplet components are always substantially narrower than the typical F-band breadths of 0.2 eV. The narrow component bands do *not* imply that the electron-lattice interaction in these F centers is weaker than in other alkali halides. (It may also be noted that similar effects occur commonly in other color centers, the F_A center being one particularly clear example.)

Complementary to the narrowing is an enhanced splitting of the centroids of the $P_{1/2}$ and $P_{3/2}$ bands beyond the static-lattice value of $\frac{3}{2}\lambda$. This effect, emphasized by HSS, arises from the manner in which the upper and the two lower energy sheets are repelled from each other as Z and T increase. It is also reflected in Eq. (3e), where it was remarked that $\langle E^2\rangle_3$ and $\langle E^2\rangle_5$ are independent of λ. Since the effect of the spin-orbit coupling is to cause the component bands to narrow, part of the value of $\langle E^2\rangle_3+\langle E^2\rangle_5$ must be made up by increasing the splitting of the $P_{1/2}$ and $P_{3/2}$ centroids beyond $\frac{3}{2}\lambda$. This effect also has been observed in the CsCl and CsBr F centers, where the $P_{1/2}$ and $P_{3/2}$ component splittings are larger than the value of $\frac{3}{2}\lambda$ derived from a moments analysis by HSS of the circular dichroism results of Margerie and Romestain.[2]

The effects of Γ_{3g} and Γ_{5g} electron-lattice coupling on the degenerate electronic states $|i\rangle|m\rangle$ are, of course, Jahn-Teller effects. Moran's treatment is in effect an adiabatic treatment of the Jahn-Teller effect for the F center. In the large spin-orbit splitting limit the effect of the Z and T interactions on the $P_{3/2}$ state is the same problem as was treated by Longuet-Higgins *et al.*,[15] and Moran's treatment is an adiabatic approximation to their fully quantized treatment of the vibrational modes. The two treatments have similar qualitative results, both predicting a splitting of the absorption band into a doublet. The adiabatic approach, however, predicts a symmetric band, whereas the treatment of Longuet-Higgins *et al.* results in the high-energy band being somewhat narrower and weaker than the low-energy band, even for vibrational frequencies as small as 1/15 of the bandwidth. Also note that the narrowing and enhanced splitting of the $P_{1/2}$ and $P_{3/2}$ bands are two of the phenomena known as "spin-orbit stabilization of the Jahn-Teller effect."

[15] H. C. Longuet-Higgens, U. Öpik, M. H. L. Pryce, and R. A. Sack, Proc. Roy. Soc. (London) A244, 1 (1958).

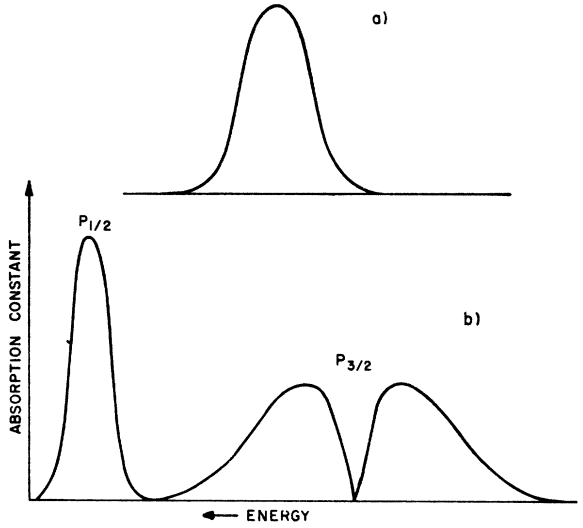

FIG. 3. Line shapes on the Moran model for the cases (a) $\lambda \ll W_3$ and (b) $\lambda \gg W_3$.

C. Effect of Γ_{1g} Mode Coupling

We now consider the Γ_{1g} mode, corresponding to the parameter S. The effect of this mode upon $f(E)$ depends upon the value of W_1^2, the second moment of the probability distribution of S. We could treat S on the same footing as Z and T, effectively adding another dimension to Figs. 2(a) and 2(b). However, a better way to include the effect of S is to note that $S\mathcal{O}_1$ is diagonal in all representations, be they $|j,m_j\rangle$, $|i\rangle|m\rangle$, or whatever. Consequently, S affects the line shape $f(E)$ in a particularly simple way, as follows.

Let $f_c(E)$ be the line shape computed by setting $W_3=\lambda=0$ and $W_1=W_{10}\neq 0$, and let $f_N(E)$ be the line shape for $W_1=0$, $\lambda=\lambda_0\neq 0$, and $W_3=W_{30}\neq 0$, as before. Let both $f_c(E)$ and $f_N(E)$ have unit areas and centroids $\langle E\rangle$. Then for $W_1=W_{10}$, $W_3=W_{30}$, and $\lambda=\lambda_0$ the line shape $f(E)$ is

$$f(E)=\int d\epsilon\, f_c(\epsilon+\langle E\rangle) f_N(E-\epsilon)\,, \tag{7}$$

a simple convolution of $f_c(E)$ and $f_N(E)$. In Moran's treatment the triplet line shape $f_N(E)$ would be folded into a Gaussian of second moment W_1^2, giving rise to a broadening and washing out of the structure. For $W_1>\lambda$ the Gaussian shape of $f_c(E)$ would dominate $f(E)$ even if $\lambda>W_3$.

An important point for the CsF F center is that Eq. (7) for $f(E)$ is not restricted to an adiabatic model. The same separation between $f_c(E)$ and $f_N(E)$ would occur in a full-fledged quantum treatment of the Hamiltonian (1). In this case $f_c(E)$ would be the $f(E)$ resulting if the a_k corresponding to the Γ_{3g} and Γ_{5g} modes are set to zero and those for the Γ_{1g} modes left unchanged, whereas $f_N(E)$ corresponds to the opposite choice. Equation (7) applies to this case as well.

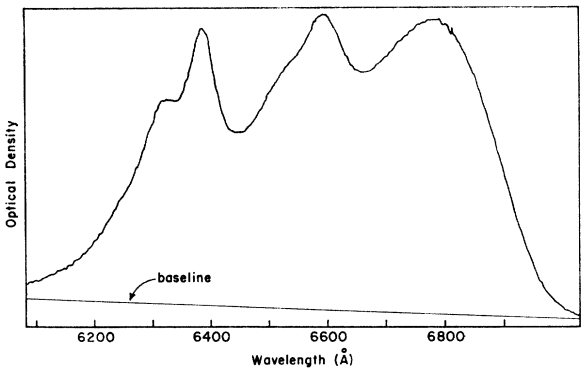

FIG. 4. F band of CsF at 15°K.

This fact permits us to extend the Moran model by using an adiabatic treatment for $f_N(E)$ and a quantized treatment for $f_e(E)$. The latter is just the same as the usual treatment of optical absorption between two electronic singlet levels subjected to a linear electron-phonon coupling, and will be sketched in Sec. IV in the actual application.

D. Circular and Stress-Induced Dichroism

Circular dichroism refers to the situation in which the $f(E)$ observed for two different senses of circularly polarized light differ. It is usually observed for light propagating along the direction of an applied magnetic field and in the F center results from unequal spin polarization in the ground state and spin-orbit coupling in the excited state. (We neglect the relatively small Zeeman effects in the excited state.) In the adiabatic model the line shapes for the two polarizations can be computed just as described for the unpolarized line shape, using the usual transition probabilities between the states $|0\rangle|m\rangle$ and $|j,m_j\rangle$.

As previously mentioned, the change in first moment in the circular dichroism is independent of H_{eL}. Consequently, the enhanced splitting of the $P_{1/2}$ and $P_{3/2}$ bands beyond $\frac{3}{2}\lambda$ by the noncubic terms of H_{eL} will be accompanied by a reduction in the magnitude of the circular dichroism for the bands below the static lattice values, so that, e.g., the absorption constant in the $P_{1/2}$ band does not go to zero for complete spin polarization and a particular circular polarization, as it would in the static lattice.

In stress-induced dichroism similar effects occur. The application of uniaxial stress causes the line shape measured with the light polarized alternately perpendicular and parallel to the stress to differ [the line shapes are denoted $g_\perp(E)$ and $g_\parallel(E)$]. A full-fledged moment analysis of $g_\parallel(E)-g_\perp(E)$ for [100] and [110] stresses, such as made by Schnatterly,[6] can be made to yield $\langle E^2\rangle_3$ and $\langle E^2\rangle_5$ individually. The experiments here are more modest, being restricted to [100] stresses, and serve mostly to show the qualitative effect of stress on the line shape. The strong spin-orbit coupling causes the line shape to alter by trading oscillator strength from one part to another, rather than by shifting rigidly, a situation similar to the dynamic stress problem. As for the circular dichroism, the change in first moment is independent of H_{eL}. The adiabatic model may be used to predict the shapes of $g_\perp$ and $g_\parallel$ just as for the unperturbed line shape.

III. EXPERIMENT

A. Sample Preparation

The experiments on optical absorption, circular dichroism, and stress-induced effects were performed on colored specimens of CsF of rectangular shape with typical dimensions of a few millimeters on a side. These were cleaved from single-crystal pieces supplied by the Harshaw Chemical Co. or Semi-Elements Inc. Although CsF is quite deliquescent, the use of a drybox for cleaving and mounting the samples in a cryostat proved adequate to provide unclouded sample surfaces for the optical work. The uncolored crystals varied in optical quality from clear to cloudy.

The coloring procedure proved to be somewhat troublesome. Additive and electrolytic coloration techniques, although they have been used on CsF, are difficult due to the deliquescence. Coloring by x irradiation was therefore adopted. The spectra produced by x irradiation were generally sample-dependent, although some bands, and in particular the prominent F band, were present in all samples. In certain samples bands occurred which overlapped the F band, distorting its shape (in some cases severely). It was found empirically

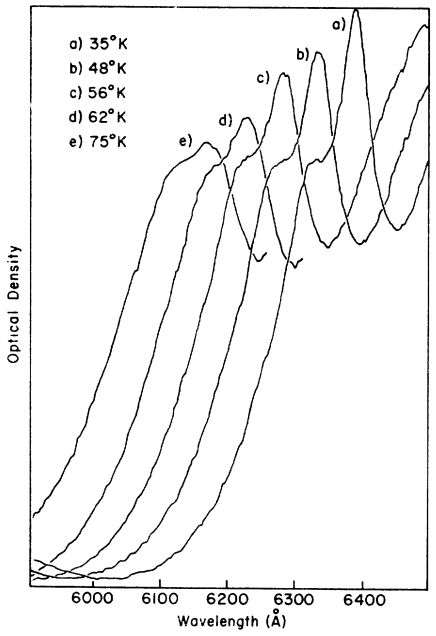

FIG. 5. Temperature dependence of the substructure. Successive curves are displaced by 50 Å for clarity.

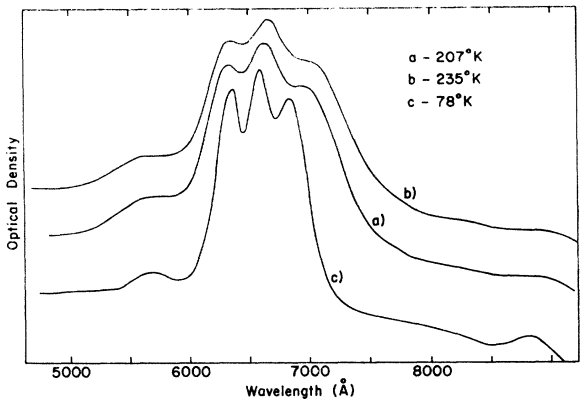

FIG. 6. Temperature dependence of the F band and K band above 80°K.

that x irradiation at liquid-nitrogen temperatures of samples cleaved from Harshaw material generally produced spectra largely free of these extraneous absorptions. Such overlapping bands as did occur could frequently be optically bleached, and usually had initial optical densities less than 10% that of the F band. In general, the results reported below are determined for samples in which the F band shape was not seriously distorted by these extraneous absorptions.

B. Optical Absorption Spectra

Optical absorption spectra were recorded on a Cary 14 R spectraphotometer using an optical cryostat of standard design. Figure 4 shows a trace of the low-temperature F band of CsF. The line shape is typical of those observed in samples free of background absorptions for temperatures lower than 30°K. The following features of the line shape are of interest: There is an over-all triplet structure with components peaking at 6390, 6600, and 6780 Å, the individual components being 550–650 cm^{-1} (0.07–0.08 eV) wide. In addition the central and high-energy peaks have structure of their own. The central peak is a weak doublet while the high-energy peak has a sharp peak at 6390 Å, a well-defined shoulder at 6340 Å, and a break in slope at 6280 Å. This latter feature is difficult to see but is clearly present in the original data. The apparent energy separation of the structure components is about 150 cm^{-1} (0.02 eV). The structure in Fig. 4 is better resolved than in the line shape originally seen by Hughes and Rabin,[11] in which only the triplet and a hint of the high-energy shoulder were visible. This difference is probably due to the sample-preparation problems previously mentioned.

C. Optical Absorption–Temperature Dependence

From 1.3 to ≈40°K the line shape is temperature-independent. The changes occurring at higher temperatures are shown in Figs. 5 and 6. Up to ≈80°K the major changes take place in the substructure (Fig. 5). With increasing temperature the sharp peak at 6390 Å diminishes in height relative to the rest of the high-energy peak and becomes unresolved at about 80°K. The break in slope at 6280 Å and the doublet structure of the central peak become washed out at about 60°K, while the band as a whole broadens and decreases in height. This trend continues in Fig. 6, which shows absorption curves (for a different sample) at and above liquid-nitrogen temperature. The low-energy component shows a particularly large red shift and broadening with increasing temperature. The central peak has a smaller red shift and the high-energy peak has no noticeable shift. The entire F band shifts to the red by about 0.03 eV from helium temperature to 234°K.

D. K Band

"K band" is the commonly accepted name for a small band which appears just to the high-energy side of the F band in various alkali halides. It is thought to arise from transitions to one or more of the higher excited states of the F center. In CsF the analogous band is very well resolved from the F band (Fig. 6) and is centered at 5700 Å at low temperatures. The area of the K band is temperature-dependent, increasing with increasing temperature, as may be seen in Fig. 6.

E. Circular Dichroism

The absorption spectra denoted $\alpha_+(E)$ and $\alpha_-(E)$ in Fig. 7 were measured using conventional techniques for a sample of colored CsF immersed in liquid He at 1.43°K. These spectra show the F band for two opposing directions of an applied 8400-G magnetic field and for circularly polarized light propagating in the field direction. The two spectra differ (circular dichroism), the high-energy peak being suppressed and the central and low-energy peaks being enhanced for one sense of the field, and vice versa for the opposing sense. The change in absorption constant is substantial, $\alpha_+/\alpha_- \approx 1.5$ in the neighborhood of the high-energy peak. The effect is temperature- and magnetic-field dependent, and qualitatively speaking is only observed for temperatures

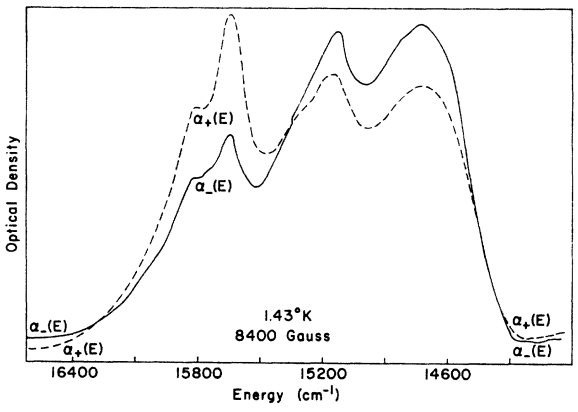

FIG. 7. $\alpha_+(E)$ and $\alpha_-(E)$, the circular dichroism spectra.

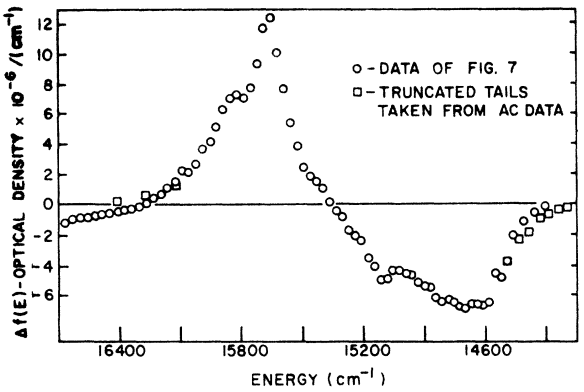

FIG. 8. $\Delta f(E)=[\alpha_+(E)-\alpha_-(E)]/E$.

T and magnetic fields H for which $\mu_\beta H$ is of order kT (μ_β is the Bohr magneton), suggesting that the effect arises from ground-state spin polarization, as was anticipated. For $g=2$ this temperature and field correspond to $\langle S_z\rangle_+=-0.187$.

For the moments analysis of the circular dichroism the function $\Delta f(E)=(\alpha_+(E)-\alpha_-(E))/E$ is required. Since the third moment of this function is important in the analysis it is necessary to know $\Delta f(E)$ in the tails of the F band with reasonable accuracy. The data of Fig. 7 are not adequate for this purpose since the tails of $\alpha_+(E)$ and $\alpha_-(E)$ do not match, due to small drifts in the measuring apparatus during the course of the measurement. To correct for this, the circular dichroism in the tails of the band was measured more accurately using an ac rotating circular polarizer technique similar to that of Henry.[4] These measurements are used to extend the $\Delta f(E)$ curve derived from $\alpha_+(E)$ and $\alpha_-(E)$. The resulting $\Delta f(E)$ is shown in Fig. 8.

The moments of $f(E)$ and $\Delta f(E)$ required for an HSS analysis of the circular dichroism are extracted from the curves of Figs. 4 and 8 and are

$$\langle E\rangle=15\,208\pm10\ \text{cm}^{-1},$$
$$\langle E^2\rangle=234\,400\pm1000\ \text{cm}^{-2}=(484\pm1\ \text{cm}^{-1})^2,$$
$$\Delta A/|\Delta A|=0.03\pm0.1,$$
$$\Delta\langle E\rangle_+-\Delta\langle E\rangle_-=105\pm5\ \text{cm}^{-1},$$
$$\Delta\langle E^2\rangle_+-\Delta\langle E^2\rangle_-=14\,100\pm2000\ \text{cm}^{-2},$$
$$\Delta\langle E^3\rangle_+-\Delta\langle E^3\rangle_-=(4.28\pm0.4)\times10^7\ \text{cm}^{-3},$$

where $|\Delta A|$ is the area under the curve $|\Delta f(E)|$. The quoted uncertainties in the moments of $f(E)$ are based on the possible errors in the choice of baseline in Fig. 4, while those quoted for the lower moments of $\Delta f(E)$ are based on the drifts in the measuring apparatus which cause the displacement of the tails of $\alpha_+(E)$ and $\alpha_-(E)$ in Fig. 7. The uncertainty quoted for the third moment of $\Delta f(E)$ is based on estimates of the possible error involved in matching the ac data taken for the tails of $\Delta f(E)$ to the rest of the curve.

In the course of the ac circular dichroism measurements some information was obtained concerning the ground-state spin-lattice relaxation time. These measurements were carried out with the sample in exchange gas in contact with a pumped liquid-helium bath, so that with a small heater on the sample holder one could increase the sample temperature above ambient. After switching off the heater the sample would cool to its equilibrium temperature in $\approx\frac{1}{2}$ sec. It was observed that for a field of 36 kG the circular dichroism of the sample, which was unobservable at the initial (heater on) temperature of ≈30°K reached its full value within the cooling time of $\frac{1}{2}$ sec upon switching the heater off (final temperature ≈2.1°K). Under these conditions, then, the spin-lattice relaxation time is less than this.

F. Stress-Induced Effects

The effect of both hydrostatic and uniaxial stress on the CsF F band were investigated. The hydrostatic pressure experiment made use of a beryllium-copper optical pressure cell with sapphire windows using helium gas as a pressurizing agent.[16] Optical absorption spectra of the sample at liquid-nitrogen temperature at pressures of 3830 and 0 atm are shown in Fig. 9. The F band shifts slightly to *lower* energies under pressure, the coefficient being $(-1.0\pm0.1)\times10^{-4}$ eV kg/mm^2. The shift is nearly a rigid one although the dips between the three peaks becomes slightly more shallow, the difference in absorption constant between the peaks and the dips decreasing by about 5%. Also, the area of the band is decreased by about 10% at the higher pressure.

The effect of an applied [100] uniaxial stress in producing a dichroism for linearly polarized light in the CsF F band was investigated using the rotating-polaroid technique of Schnatterly.[5] Figure 10 shows the difference in the absorption constant for light polarized parallel and perpendicular to the stress direction, for the CsF F band at nitrogen temperature. Two points are interesting in this spectrum. First, the curve is not

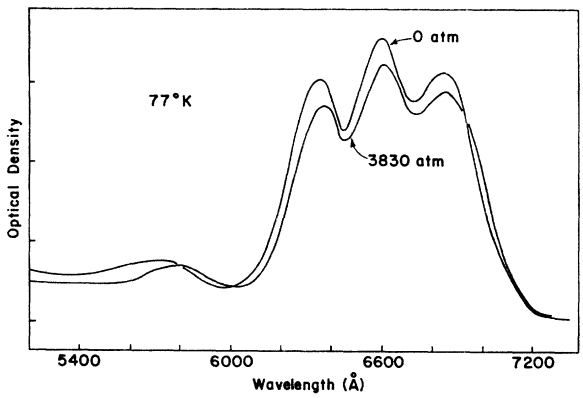

FIG. 9. Effect of hydrostatic pressure on the CsF F band.

[16] D. B. Fitchen, Rev. Sci. Instr. 34, 673 (1963).

what would be obtained from a rigid shift of the line shape in energy between the two polarizations, but rather indicates that the higher-energy peak, and to a lesser extent the central peak, grow at the expense of the low-energy peak, with none of the peaks shifting. Second, the magnitude of the effect is large by F band standards, amounting to a change in optical density of about 3% at the wavelength at which the effect was largest for an applied stress of 1 kg/mm^2. The centroids of the two spectra differ by an amount corresponding to a shift in the line-shape functions of $(2.1\pm0.4)\times10^{-3}$ eV/(kg/mm^2), with the error reflecting the accuracy to which the stress is known.

A single investigation of the stress-induced dichroism at helium temperatures was made by simply recording $\alpha(E)$ on the Cary spectraphotometer for light polarized parallel and perpendicular to the stress direction. The results were similar to the nitrogen-temperature behavior, the central and high-energy peaks alternately growing and shrinking at the expense of the low-energy peak, with no noticeable shift in peak positions. The substructure of the high-energy peak retained their relative proportions in this change. The magnitude of the effect was an approximately 10% change in optical density between the two polarizations for an applied stress of 3 kg/mm^2, approximately the same as at nitrogen temperatures.

IV. ANALYSIS

A. Low-Temperature Line Shape

The interpretation of the experimental line shape is guided by analogies with other F centers, especially those of the cesium halides. Since the circular dichroism behavior is similar to that of the F bands in CsBr and CsCl[2], the same model is adopted, namely, a transition from the usual F-center S-like ground state to a set of P-like excited states split by spin-orbit coupling. The high-energy component band is assigned to the $P_{1/2}$ level and the others to the $P_{3/2}$ level because they display the opposite sense of dichroism and have proportionally correct areas ($P_{1/2}$ having higher energy than $P_{3/2}$ is typical of F centers).

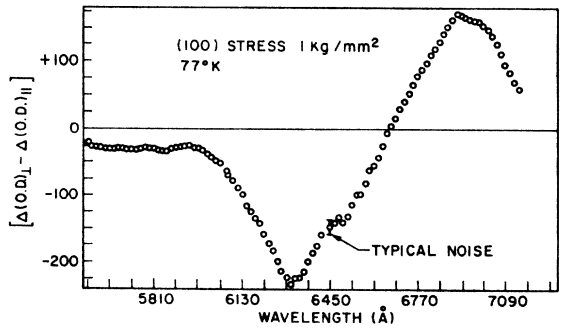

FIG. 10. Uniaxial-stress-induced dichroism at 77°K. The quantity plotted (in arbitrary units) is the change in optical density times 10^4 and is proportional to $E[g_\perp(E)-g_\parallel(E)]$.

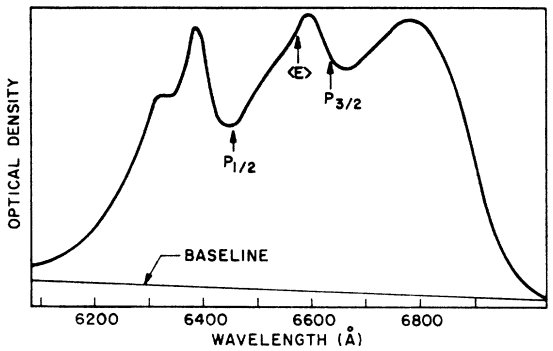

FIG. 11. F band in CsF after Fig. 4 with the positions of the static lattice $P_{1/2}$ and $P_{3/2}$ points indicated.

To further interpret the line shape we can use the Moran model and an HSS moments analysis of the circular dichroism. The situation is complicated by the presence of the substructure, which does not fit into such an analysis in an obvious way. However, we will follow the procedure of initially accepting the substructure as an unexplained feature whose source is nevertheless to be found in the Hamiltonian (1). This permits use of the HSS results (4) in interpreting the circular dichroism. It turns out that the results of this analysis suggest, and in fact virtually require, that the substructure be interpreted in terms of discrete phonon structure, thus fitting into the Hamiltonian as it stands. It can further be argued that such effects are to be expected in CsF.

The well-resolved, narrow triplet structure of the low-temperature line shape shown in Fig. 4 indicates on the Moran model that the electron-lattice coupling to Γ_{3g} and Γ_{5g} modes is comparable in strength to the spin-orbit coupling, and that the electron-lattice coupling to the Γ_{1g} modes is relatively weak. Moran's values of λ, W_1^2, and W_3^2 based on a fit to the line-shape data on Hughes and Rabin were in fact $\lambda=-267$ cm^{-1}, $W_1^2=(175\text{ cm}^{-1})^2$, and $W_3^2=(260\text{ cm}^{-1})^2$.

These numbers may be compared with those derived from the circular dichroism as computed from (4) and the moments of $f(E)$ and $\Delta f(E)$, using $\langle S_z\rangle=0.187$. These give $\lambda=-280\pm15$ cm^{-1},[17] $\langle E^2\rangle_3+\langle E^2\rangle_5=157\,000\pm27\,000$ cm$^{-2}=(397\pm25\text{ cm}^{-1})^2$ and $\langle E^2\rangle_1=37\,000\pm27\,000$ cm$^{-2}=(194_{-90}^{+50}\text{ cm}^{-1})^2$. Making the identification $W_1^2\sim\langle E^2\rangle_1$ and $W_3^2\sim\langle E^2\rangle_3+\langle E^2\rangle_5$, these experimental values agree with Moran's predictions. We shall show subsequently that for these parameters the Moran model actually predicts a line shape somewhat at variance with the experimental line shape, so that the apparent agreement is partially accidental and the result of an approximation made by Moran. Nonetheless, the basic idea of weak Γ_{1g} mode coupling and strong spin-orbit and Γ_{3g} and Γ_{5g} mode coupling is borne out by the circular dichroism results. Also note the narrow

[17] An earlier value of $\frac{3}{2}\lambda=340$ cm^{-1} given in T. A. Fulton and D. B. Fitchen, Bull. Am. Phys. Soc. 11, 245 (1966) is wrong.

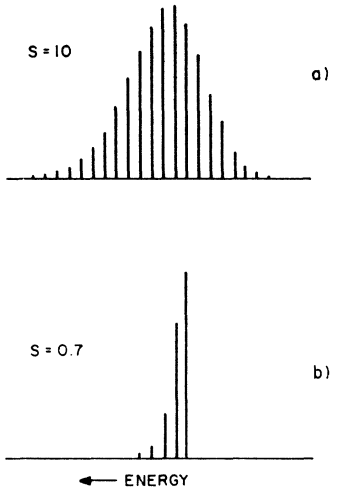

FIG. 12. $f_c(E)$ for a single Γ_{1g} mode with (a) $S=10$ and (b) $S=0.7$.

widths and the related enhanced splittings of the triplet components, as shown by the position of the static-lattice $P_{1/2}$ and $P_{3/2}$ levels indicated in Fig. 11.

The relatively small value of $\langle E^2\rangle_1$ suggests the solution of the question of the source of the substructure. As pointed out in Sec. II, the effect on the line shape of coupling to the Γ_{1g} modes can be described in terms of a line shape $f_c(E)$. The actual line shape $f(E)$ is a convolution of $f_c(E)$ with the noncubic line shape $f_N(E)$ as in Eq. (7). In the Moran model, $f_c(E)$ is a Gaussian, of second moment $W_1^2=(194_{-90}^{+50}\ \mathrm{cm}^1)^2$ for CsF. In a quantized treatment $f_c(E)$ is only Gaussian, or nearly Gaussian if the phonon frequencies of the Γ_{1g} modes involved are small compared to the square root of the second moment of $f_c(E)$, so that the bulk of the transitions are multiphonon. In CsF this is *not* the case.

The computation of $f_c(E)$ is the standard one for singlet-singlet transitions with a linear electron-phonon coupling.[18] Defining the Huang-Rhys parameter $S_k=a_k^2/(2M_k\omega_k^2)$ for the kth mode, the transition probability from the ground state to the excited state having the kth mode excited to a level of n_k quanta is $\prod_k(S_k^{n_k}/n_k!)e^{-S_k}$. The line shape possesses a first moment E_1-E_0 independent of the S_k and a second moment $\sum_k S_k(\hbar\omega_k)^2$. An approximation frequency used is to attribute all the electron-lattice interaction to a single mode of frequency ω with Huang-Rhys factor S. In this approximation $f_c(E)$ consists of a series of line shapes spaced $\hbar\omega$ apart. The first moment of the band is again E_1-E_0 and the second moment is $S(\hbar\omega)^2$. The intensity of the line at energy $E_1-E_0-(s-n)\hbar\omega$ where $n=0, 1, 2, \cdots$ is proportional to $(S^n/n!)e^{-S}$. This expression peaks, for large S, at approximately $n=S$, so that S is often called the most probable number of phonons released in the optical transition. For large S the line shape is approximately Gaussian. Figure 12 shows schematically the line shapes of the single-mode coupling model for a large and a small value of S.

The phonon energies and densities of states in CsF are unusual for alkali halides as a result of the large CsF mass ratio. One would expect a sizable gap between the optical and acoustic modes on this account, an expectation borne out by the calculations of Hardy and Karo.[19] They find that the acoustic phonons occur dominantly in and around 40 cm^{-1} and the optical phonons at 150 cm^{-1}, with a sizable gap between the two branches. If we now consider the $\langle E^2\rangle_1=(194_{-90}^{+50}\ \mathrm{cm}^{-1})^2$ for CsF in comparison with the expression $\sum_k S_k(\hbar\omega_k^2)$ for the second moment of $f_c(E)$, we see immediately that the value of $\sum_k S_k$, summed only over the Γ_{1g} optic modes, can only be at most 1 or 2. If we further consider that the optical phonons in CsF are concentrated primarily

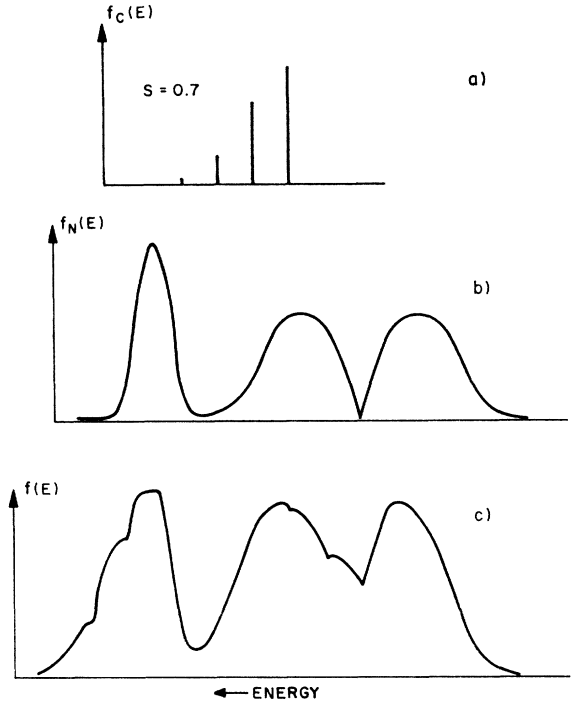

FIG. 13. (a) $f_c(E)$ for single mode with $S=0.7$; (b) typical $f_N(E)$, and (c) convolution of $f_c(E)$ and $f_N(E)$.

at one energy well away from the acoustic phonons we are lead to the conclusion that the substructure is most probably due to a weak coupling of the optical transitions to the Γ_{1g} optical phonons. To see how this can cause the substructure, consider the $f_c(E)$ which results from coupling to a single mode of frequency $\hbar\Omega$ with a Huang-Rhys parameter of 0.7, as shown in Fig. 13(a). The convolution of this line shape with that of a typical $f_N(E)$ [Fig. 13(b)] is shown in Fig. 13(c) and yields substructure of the sort seen in the experimental curve whenever $\hbar\Omega$ is comparable to the

[18] See, e.g., D. E. McCumber, J. Math. Phys. **5**, 221 (1964); 5, 508 (1964), and references therein.

[19] J. R. Hardy and A. M. Karo, Phys. Rev. **168**, 1054 (1968).

width of the peaks of $f_N(E)$. One can identify the spike, shoulder, and break in slope of the experimental high-energy peak as reflecting transitions to the $P_{1/2}$ state with the accompanying release of zero, one, and two Γ_{1g} optical phonons. Similarly, the shoulder on the central peak is the one-Γ_{1g} optical-phonon image of the central peak itself, which is a zero-Γ_{1g} optical-phonon transition. From the relative height and separation of the spike and shoulder of the $P_{1/2}$ peak the S value for the transition can be estimated to be approximately 0.7 and the frequency of the optical phonons of order 150–200 cm^{-1}.

Moran has previously calculated the line shapes of the cesium-halide F bands using his adiabatic model sketched in Sec. II. As an important approximation he assumed that the effect of the mixing between the $P_{1/2}$ and $P_{3/2}$ states caused by the Z and T distortions could be treated by perturbation theory. This assumption enabled him to compute line shapes which could reproduce with fair accuracy all the cesium-halide F bands. However, as Moran suggests, if $\frac{3}{2}\lambda$ is comparable to W_3, perturbation theory is not valid, particularly in view of the energy surfaces of Fig. 2. The Moran treatment is equivalent to initially regarding the surfaces emanating from the $P_{3/2}$ energy as cones and the $P_{1/2}$ surface as flat. The effect of the $P_{1/2}$-$P_{3/2}$ mixing is taken as adding a quadratic term to the energies, giving them a paraboloidal shape, bending away from each other. As Fig. 2 shows, this would only be a good approximation if Z and T were confined to excursions of $\frac{1}{4}\lambda$ or less, which is not the case for any of the cesium halides.

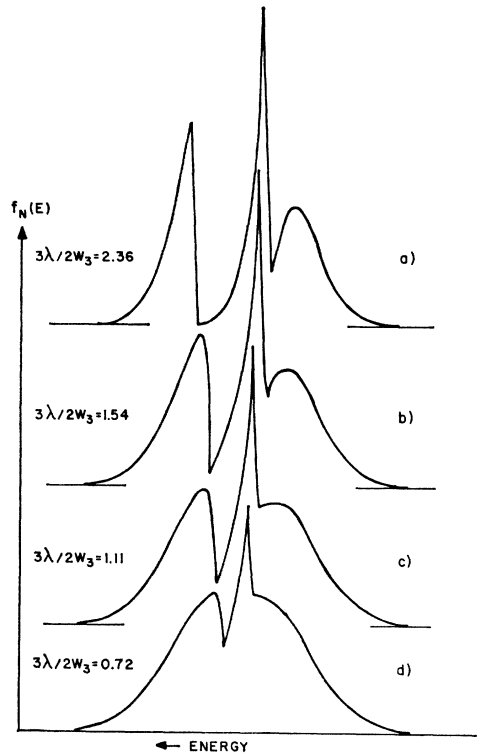

FIG. 14. Computer calculation of $f_N(E)$ from the Moran model for several values of $3\lambda/2W_3$.

We have numerically calculated the line shapes predicted by Moran's treatment using exact diagonalization of the matrix resulting from (5), a task made simpler by recognizing that one may first set $S=0$ and calculate $f_N(E)$ (two variables only) and then convolve it with $f_c(E)$ subsequently to produce $f(E)$. Further, one may choose either a Gaussian for $f_c(E)$, as in the adiabatic treatment, or something akin to Fig. 12(b), which is more suitable for CsF.

In Fig. 14 we show the shapes of $f_N(E)$ calculated for several values of $3\lambda/2W_3$. Even for $3\lambda/2W_3=2.36$ these curves are still quite unlike those predicted by the perturbation approach. Using the $\frac{3}{2}\lambda=420$ cm^{-1} and the $\langle E^2\rangle_3+\langle E^2\rangle_5=(397\pm25$ $cm^{-1})^2$ of the circular dichroism experiments, the line shape of Fig. 13(b) is the appropriate one for CsF. It is clear from the figure that the computed line shape disagrees with the experimental line shape of Fig. 4. Qualitatively, the expected triplet structure is present but the dip between the $P_{3/2}$ peaks is much less pronounced than the experimental dip (allowing for the cubic-made broadening) and the central peak is higher and narrower. {The sharp central peak comes from saddle points in the central energy surface [Fig. 2(a)].} Also, the $P_{1/2}$ peak is somewhat broader than the experimental $P_{1/2}$ peak (allowing again for the cubic-mode broadening). Convolving this shape with $f_c(E)$ will tend to broaden the central peak but will further wash out the dip.

Although Moran's model does not quantitatively reproduce the CsF line shape, the physical idea of the source of the $P_{3/2}$ splitting is surely correct. One may ask if an extension of the model would significantly alter the predicted line shape. We consider three possibilities.

A rather simple extension, staying within the adiabatic framework, is to include the effects of more than one Γ_{3g} mode. In this case the Hamiltonian (5) would contain a sum of terms $\sum_i (T_i \mathcal{O}_{3a}+Z_i \mathcal{O}_{3b})$, each Z_i and T_i having its own Gaussian probability distribution with second moment W_{3i}^2. The effect of these terms is clearly the same as that of a term $T' \mathcal{O}_{3a}+Z' \mathcal{O}_{3b}$, where $T'=\sum_i T_i$ and $Z'=\sum_i Z_i$ have Gaussian probability distributions of second moment $\frac{1}{2}W_3'^2=\sum_i \frac{1}{2}W_{3i}^2$. The effect of several Γ_{3g} modes is therefore equivalent to that of a single Γ_{3g} mode with a properly chosen W_3.

Another possible improvement is to include the effect of a Γ_{5g} mode, still in an adiabatic approximation. This involves adding to the Hamiltonian (5) the terms $\xi \mathcal{O}_{5a}+\eta \mathcal{O}_{5b}+\zeta \mathcal{O}_{5c}$, where $\mathcal{O}_{5a}=\sqrt{3}(|x\rangle\langle y|+|y\rangle\langle x|)$ corresponds to a strain of xy symmetry and $\mathcal{O}_{5b}$ and $\mathcal{O}_{5c}$ are similar expressions for yz and zx strains. ξ, η, and ζ have Gaussian probability distributions with second

moments $\frac{1}{2}W_5^2$. Moran pointed out that for $W_5 \ll W_3$ the effect of the Γ_{5g} modes may be simulated by increasing the value of W_3^2 to $W_3^2+W_5^2$. If $W_3 \approx W_5$, an accurate treatment can only be made by diagonalizing the full 6×6 matrix of the Hamiltonian for the states $|j,m_j\rangle$, a problem beyond our analytical powers or computational budget. However, if $\lambda \gg W_3$ and W_5, the $P_{1/2}$ state can be ignored and the matrix reduces to a 4×4 representing the effect of combined Γ_{3g} and Γ_{5g} strains on a $P_{3/2}$ state. The solution of the eigenvalue problem is then

$$\epsilon = E_1 - E_0 + \tfrac{1}{2}\lambda \pm (Z^2+T^2+\xi^2+\eta^2+\zeta^2)^{1/2},$$

each level being a Kramers doublet. The exact shape of the $P_{3/2}$ band depends on the relative values of W_3 and W_5 although it is in all cases a doublet. In general, the dip between the two components is increasingly scooped out for increasing ratios of W_5/W_3, the maximum effect being at $W_5=W_3$ where the phase space is effectively five dimensional. Correspondingly, the peaks narrow somewhat so as to preserve the total second moment.

For W_3 and W_5 comparable to λ we can only be qualitative. It seems probable that the dip between the $P_{3/2}$ components will remain deeper than for Γ_{3g} coupling alone. Also, the central peak will again be narrower and taller than the low-energy peak since this occurs as a result of interactions between the $P_{1/2}$ level and the upper strain-split $P_{3/2}$ level. The general effect of Γ_{5g} coupling would be to produce a line shape somewhat closer to the experimental, chiefly in that the dip between the $P_{3/2}$ components would be more pronounced.

Finally, we note that in the treatment of Longuet-Higgins *et al.*,[15] the high-energy peak is substantially weaker and narrower than the low-energy peak, whereas the adiabatic treatments give peaks of equal areas. A revision of this sort would improve the fit to the line-shape data.

B. Temperature Dependence

The temperature dependence of the substructure (Fig. 5) is not fully understood. In general, the resolution of $f(E)$ into $f_c(E)$ and $f_N(E)$ should be valid at all temperatures, so that the substructure should display the temperature dependence of $f_c(E)$. However, for the small value of $S=0.7$ and the phonon energies of 150 cm^{-1} one would not expect any substantial change in $f_c(E)$ from optical phonons for temperatures as low as 80°K. The acoustic phonons, concentrated around 40 cm^{-1}, might be expected to have some effect at this temperature but their effect should be restricted to shifting oscillator strength through 40 cm^{-1} or so, which should merely broaden the substructure, whereas the spike at 6390 Å in Fig. 5 shows an apparent sharp decrease in oscillator strength. It is probable that the underlying temperature dependence of $f_N(E)$ is confusing the issue.

For temperatures above 80°K the line shape has a temperature dependence (Fig. 6) which can be understood on the Moran model with the additional assumption of a mixing (and hence a repulsion) between the K-band levels and the $P_{1/2}$ and $P_{3/2}$ levels. On the Moran model confined to the P levels, one anticipates that at high temperatures the high- and low-energy tails of the F band should be mirror images, at least for energies large compared to the spin-orbit splitting. Also, the centroid of the F band should remain fixed. (Shifts from thermal expansion of the lattice are negligible because of the very small pressure coefficient.) Neither of these features is found experimentally. However, since the K band is increasing in area with increasing temperature it seems likely that there is a mixing with the P and K levels which effects the $P_{1/2}$ level primarily, since it lies closest in energy to the K levels. It is effectively "pinned" in place between the K levels and the $P_{3/2}$ levels, and thus is less broadened with increasing temperature, an effect similar to that which causes the central peak of the F band at low temperatures to be substantially sharper than the low-energy peak. The increasing area of the K band with temperature goes along with the shift of the F band to lower energies in such a way as to hold the K band $+F$ band centroid fixed. The experimental data in Fig. 6 suggest that the centroid is indeed fixed, although variations in background preclude quantitative checks of this point.

The behavior of the low-energy peaks with increasing temperature can be understood from the energy curves of Fig. 2. The low-energy sheet decreases in energy with increasing T and Z, so that the low-energy peak must red shift as the thermal excursions of T and Z increase. Also, the energy surfaces grow substantially steeper for large Z and T, accounting for the pronounced broadening. The zero-point vibrations correspond to relatively flat energy surfaces (the influence of the spin-orbit coupling) while at large T and Z the energy surfaces are almost the same as for $\lambda=0$. Also, note that the three peaks remain resolved up to room temperature, which reflects in part the fact that the $P_{1/2}$ peak and the lower $P_{3/2}$ component alternately blue and red shift (ignoring K mixing) leaving the central peak to fill in the dips, and in part the weak Γ_{1g} mode coupling.

Finally, the greatly enhanced $P_{3/2}$ splitting with increasing temperature is good support for Moran's picture of a dynamic Jahn-Teller splitting of the $P_{3/2}$ state. It suggests that the effect of the lattice vibrations on the splitting is strong and hence the zero-point vibrations are enough to provide the low-temperature splitting.

C. Stress Dependence

The hydrostatic pressure shift $(-1.0\pm0.1)\times10^{-4}$ eV/(kg/mm^2) is opposite in sign to those of other F centers, although much smaller in absolute value. The reasons for this are not entirely clear, although Buchen-

auer and Fitchen[20] have determined that the pressure shifts of the F bands of RbF and KF show a decreasing trend, and have suggested that a correlation can be made with cation and anion radii in the pressure shifts of the F band of all the alkali halides.

The [100] uniaxial stress-shift coefficient $(2.1\pm0.4)\times10^{-3}$ eV/(kg/mm^2) is substantially larger than any measured previously in the alkali halides. The large disparity between the [100] uniaxial and the hydrostatic stress-shift coefficients is similar to, but more pronounced than, the difference between $\langle E^2\rangle_1$ and $\langle E^2\rangle_3+\langle E^2\rangle_5$ and probably has the same underlying cause.

The shape of the uniaxial-stress-induced dichroism curve of Fig. 10 is in agreement with the spin-orbit split P-state model for the excited states. As mentioned in Sec. II, the $P_{1/2}$ peak does not shift but simply trades oscillator strength with the rest of the band. The fact that the central peak has a dichroism of the same sign as the $P_{1/2}$ peak and opposite from that of the low-energy peak can also be predicted from the Moran picture.

V. SUMMARY

The conclusions of this work may be summarized as follows: The F band possesses a well-resolved triplet structure with a substructure in the individual peaks. The circular dichroism shows that the P states are split by a spin-orbit coupling corresponding to a static lattice splitting of -420 ± 25 cm^{-1}, and that the coupling to Γ_{1g} modes of vibration is relatively weak and the coupling to Γ_{3g} and Γ_{5g} modes relatively strong, their respective contributions to the second moment of the line shape being $\langle E^2\rangle_1=37\,000\pm27\,000$ (cm^{-1})^2 and $\langle E^2\rangle_3+\langle E^2\rangle_5=157\,000\pm27\,000$ (cm^{-1})^2. The high-energy triplet component corresponds to the $P_{1/2}$ state and the two lower-energy components to the $P_{3/2}$ state, the latter being split by a dynamic Jahn-Teller effect as suggested by Moran. The stress-induced behavior and temperature dependence of the line shape can be understood on this model.

The interplay between the spin-orbit coupling and the Jahn-Teller effects is reflected both in the splitting of the $P_{3/2}$ band into a doublet and the enhanced splitting of the $P_{1/2}$ and $P_{3/2}$ bands beyond their static-lattice separation and the complementary narrowness of the individual triplet components.

The additional substructure of the triplet components is found to be due to optical transitions in which zero, 1, etc., optical phonons of Γ_{1g} symmetry are created. The Huang-Rhys factor is estimated to be $S\approx0.7$ and the energy of the phonons 150–200 cm^{-1}. Phonon structure is observable in CsF because of the suppression of the Γ_{3g} and Γ_{5g} broadening by the spin-orbit effect, combined with the small value of $\langle E^2\rangle_1$ and the relatively large gap between optic and acoustic phonons in CsF due to the large mass ratio.

The features of the line shape, which appear so unlike those of other F bands, occur naturally as the result of the particular coupling limit represented by CsF, namely, large spin-orbit coupling, large noncubic-mode coupling, and small cubic-mode coupling. It should not be thought that CsF is completely anomalous in possessing these particular couplings. For example, KI has a larger spin-orbit coupling but has too much cubic-mode interaction[6] to show an extreme line shape. KBr has proportionally as great a disparity in the values of $\langle E^2\rangle_1$ and $\langle E^2\rangle_3+\langle E^2\rangle_5$, but favoring the cubic coupling in that case.[6] CsCl has comparable values of $\langle E^2\rangle_1$ and $\langle E^2\rangle_3+\langle E^2\rangle_5$ but the spin-orbit splitting there[7] is only 300 cm^{-1} and the structure is therefore much less well resolved. CsF happens to have just the right mixture of coupling to produce the striking behavior that it displays and which makes it one of the most interesting of F centers.

Note added in proof. Recently, Cho [K. Cho, J. Phys. Soc. Japan **25**, 1372 (1968)] has given an approximate treatment of the adiabatic line shapes for a variety of coupling strengths for the spin-orbit and Γ_{1g}, Γ_{3g}, and Γ_{5g} electron-lattice interactions. His results overlap in part our numerical calculations of the Moran line shapes and are in good agreement in these areas. We thank Dr. Cho for bringing his work to our attention.

ACKNOWLEDGMENTS

We wish to thank the following people for helpful discussions and/or loan of equipment: Professor A. J. Sievers, Dr. L. L. Chase, Dr. L. D. Bogan, Dr. H. R. Fetterman, C. J. Buchenauer, Professor H. Mahr, Dr. D. Fröhlich, and Dr. M. D. Sturge. We thank Miss Rosemary Cox for programming the computer.

[20] C. J. Buchenauer and D. B. Fitchen, Phys. Rev. **167**, 846 (1968).